Hybrid Metasurface, Dielectric Resonator, Low-Cost, Wide-Angle Beam-Scanning Antenna for 5G Base Station Application

Zhan Wang, *Student Member, IEEE*, Yuandan Dong, *Senior Member, IEEE*, Zilin Peng, and Wei Hong, *Fellow, IEEE*

***Abstract*— This work presents a novel compact, low-cost, metamaterial-based, wide-angle beam-scanning array antenna with monopole-like Huygens pattern reconfigurable element for fifth-generation (5G) base station application. A miniaturized and broadband hybrid metasurface with a compact size of $0.28\lambda_0 \times 0.28\lambda_0 \times 0.11\lambda_0$ is first proposed by combining a dielectric resonator and a 3 × 3 mushroom-like metasurface. By exploring a monopole-like Huygens radiation mechanism, a pattern reconfigurable hybrid metasurface antenna is implemented. It can be switched between one broadside and two tilted ($\theta = \pm 40°$) modes. To increase the beam-scanning range, the proposed pattern reconfigurable antenna as the array element is adopted in a phased array. For demonstration, a five-element hybrid metasurface linear array antenna using the reconfigurable element is fabricated and measured. It is operated in the band of 3.30–3.80 GHz (5G-N78 band). This reconfigurable method can extend the beam-scanning angle of the five-element array symmetrically from [−35°, +35°] to [−70°, +70°]. With the merits of broadband, low-cost (simple design and fewer array elements), wide-angle beam-scanning capacity, and good radiation performance, the proposed hybrid metasurface pattern reconfigurable antenna and array are well poised for 5G multibeam base station and microcell applications.**

***Index Terms*— Beam scanning, dielectric resonator (DR), fifth-generation (5G) base station antenna, hybrid metasurface, metamaterial-based antenna, pattern reconfigurable antenna, phased array.**

I. Introduction

THE evolving development of fifth-generation (5G) communication technology has brought a high data rate, large channel capacity, and low-latency transmission experience to the users [1], [2]. However, multireflection and scattering are unavoidable due to the occlusion of buildings or/and trees in practical indoor and outdoor environments, which can seriously affect the link quality and robustness of 5G communication [3], as shown in Fig. 1. It is worth mentioning that multibeam antennas (such as pattern reconfigurable antenna and phased array) with the ability to improve multipath effect and dynamically switch the coverage have been considered as one of the key technologies for 5G base station applications [4], [5]. Therefore, multibeam antennas have received substantial research interest for 5G applications.

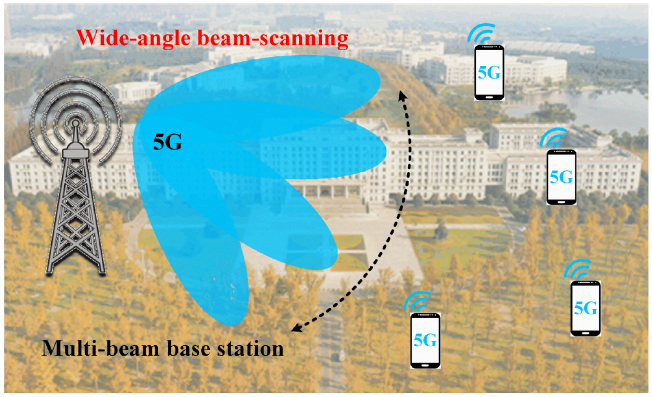

Fig. 1. 5G multibeam base station application scenario with the low-cost, wide-angle beam-scanning phased array.

Compared with the pattern reconfigurable antenna [6], the phased array not only realizes wide-angle continued beam scanning but also achieves beamforming, especially for wide-angle beam-scanning array [7]. Therefore, the phased array is widely used in radar, wireless communication, and satellite applications [7]–[9]. To broaden the beam-scanning region of the phased array, many works and efforts for the wide-angle beam-scanning array have been done in the past two decades. They can be divided into four categories [10]–[17].

1) The first method is to employ a mechanical beam scanning reflector [10]. However, the complex and heavy mechanical structures (high cost) and slow scanning speed are hard to improve.

2) The second category is to use a small radiation source with wide beamwidths, such as an electric current source and magnetic dipole [11], [12]. Although the beam-scanning angle can be obviously enhanced, they usually suffer from a narrow bandwidth and low radiation gain.

Manuscript received 29 August 2021; revised 23 March 2022; accepted 13 April 2022. Date of publication 26 April 2022; date of current version 6 October 2022. This work was supported by the National Natural Science Foundation of China under Contract 62171091 and Contract 62161160310. *(Corresponding author: Yuandan Dong.)*

Zhan Wang, Yuandan Dong, and Zilin Peng are with the School of Electronic Science and Engineering, University of Electronic Science and Technology of China, Chengdu 611731, China (e-mail: ydong@uestc.edu.cn).

Wei Hong is with the State Key Laboratory of Millimeter Waves, School of Information Science and Engineering, Southeast University, Nanjing 210096, China.

Color versions of one or more figures in this article are available at https://doi.org/10.1109/TAP.2022.3169067.

Digital Object Identifier 10.1109/TAP.2022.3169067

3) The third idea is to load the phase-shifting metasurface [13]. By refracting the electromagnetic wave, the scanning angle is widened. However, high profile, complex multilayer structure, and limited bandwidth are unavoidable.

4) The final form is to adopt the pattern reconfigurable array element. By combining the beam-scanning region for different modes (broadside and tilted beams), the pattern reconfigurable array can easily realize a wide-angle beam-scanning function [14]–[17]. Due to the limitation of the reconfigurable element, the conventional methods exhibit either a narrow bandwidth, large size, or poor radiation performance [14], [16]. Generally speaking, the abovementioned conventional designs cannot be employed in space-limited broadband 5G base station applications because of the narrow bandwidth, limited radiation capacity, large size, and complex structure (high cost). Therefore, it is desirable to develop a low-cost, wide-angle beam-scanning array with wide bandwidth and a compact size for 5G applications.

To meet the demand of the space-limited 5G base station applications, a miniaturized array element (miniaturized antenna) has been considered. Note that, usually, a small antenna realizes a wide beamwidth due to the small aperture distribution principle, which is helpful to achieve wide-angle beam scanning [18]. Also, note that metamaterials with unusual electromagnetic characteristics and novel working mechanisms have been widely adopted in miniaturized antenna designs [19]–[21]. Although the resonant-type metamaterial-based antennas have a small size, they usually suffer from a fairly narrow bandwidth [22], [23]. As a type of wide bandwidth metamaterial, the metasurface-based antenna has a large dimension that is larger than its half-wavelength, which makes it not suitable for wide-angle beam-scanning phased array design [24]. Thus, it is a big challenge but a very meaningful topic to design a metamaterial-based wide-angle beam-scanning antenna/array with a compact size and broad bandwidth for 5G base station applications.

In this article, a novel low-cost, wide-angle, beam-scanning, metamaterial-based antenna/array using five monopole-like Huygens pattern reconfigurable elements is proposed for 5G base station applications. The detailed application scenario is shown in Fig. 1.

1) By loading the mushroom metamaterial on the dielectric resonator (DR), a novel compact and broadband hybrid metasurface is first proposed.

2) A pattern reconfigurable metasurface-based antenna is then realized by etching two monopole-like vias with a p-i-n diode based on the monopole-like Huygens principle.

3) Finally, a low-cost, wide-angle beam-scanning array using five pattern reconfigurable elements is implemented and demonstrated.

II. Novel Pattern Reconfigurable Hybrid Metasurface

A. Novel Miniaturized Hybrid Metasurface

A novel miniaturized hybrid metasurface is first proposed by combining/mixing a DR and a mushroom-like metamaterial, as shown in Fig. 2. To clearly explain the working principle of the proposed hybrid metasurface, three reference designs are compared. First, a rectangular DR ($\varepsilon_r = 9.4$ and $tan\ \delta = 0.009$) is placed above the ground substrate (0.508 mm-thick F4BM substrate: $\varepsilon_r = 2.2$ and $tan\ \delta = 0.001$), which is excited by using a slot-coupled feeding structure. It is named Case 1, as shown in Fig. 2(a). Second, a metallic patch is loaded on the surface of the DR to reduce the size (Case 2), as shown in Fig. 2(b). Third, the original metallic patch is replaced by a 3 × 3 metasurface to improve the impedance matching and radiation performance, as shown in Fig. 2(c) (Case 3). Finally, four shorting vias are loaded around the surface, and a mushroom-like metasurface is loaded on the DR to enhance the impedance bandwidth, as shown in Fig. 2(d). It is marked as Case 4 (the proposed hybrid metasurface). Unlike the classical mushroom structure [24], four shorting vias are loaded in the corners of the metasurface to facilitate the implementation of the coupled feeding structure and the reconfigurable monopole-like vias with p-i-n diode bias circuits. Besides, fewer shoring vias not only obtain a larger shunt inductor but also introduce less loss [23]. Therefore, by loading fewer shorting vias on the DR, the proposed hybrid metasurface simultaneously realizes a compact size and good radiation effectively.

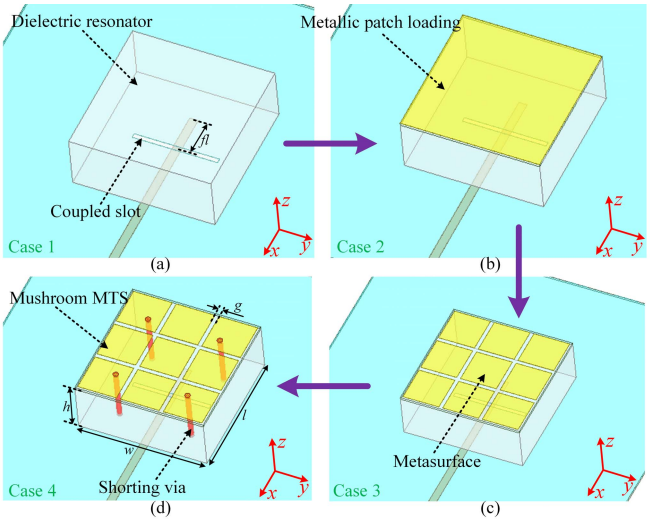

Fig. 2. Evolution of the proposed DR hybrid metasurface structure. (a) Case 1: the conventional DR with a slot-coupled feed. (b) Case 2: the DR with a metallic patch. (c) Case 3: the DR with a 3 × 3 metasurface. (d) Proposed hybrid metasurface structure with a mushroom-like metasurface. The size parameters are listed in Table I.

Fig. 3 shows the simulated $|S_{11}|$ for three reference designs and the proposed hybrid metasurface. As expected, Case 1 has a single resonant mode (TE_{111} mode), and it suffers from large size and limited bandwidth [25]. It is noted that, although the slot-coupled antenna can easily extend the bandwidth by exciting coupled slot mode, the coupled slot resonance mode is not applied due to its large back-lobe levels in this design [24]. By loading the metallic patch, the resonant frequency of Case 2 shifts to a lower region. Besides, a severe mismatching phenomenon is also observed due to the large loaded capacitance. Relying on the metasurface, although the resonant

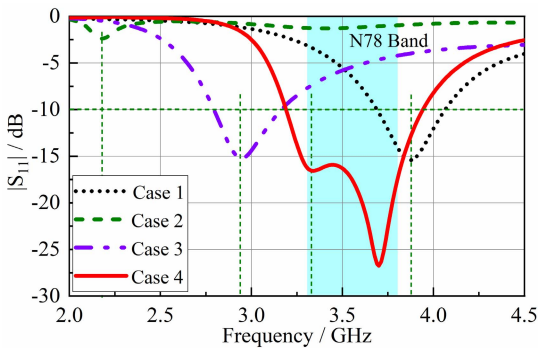

Fig. 3. Simulated reflection coefficient ($|S_{11}|$) for the antennas for different cases (Cases 1/2/3/4), as shown in Fig. 2.

frequency of Case 3 moves to a higher frequency region, the impedance matching is obviously improved compared with Case 2. This is mainly due to that the metasurface has a smaller loaded capacitance with multiple radiation slots. To balance the size and bandwidth, a mushroom-like metasurface is employed in the proposed hybrid metasurface (Case 4). A new resonant mode is generated, and a dual-mode broadband response with good impedance matching is clearly observed. Specifically, the new radiation mode (3.70 GHz) comes from the resonance of the mushroom-like metasurface [24], [26]. The resonant frequency for the DR (Case 4) slightly shifts to a high frequency (3.30 GHz). Here, the shorting vias can be considered as the extra shunt-loaded inductance. The total equivalent inductance for its equivalent resonant circuit model is then reduced. Importantly, by mixing a DR and a mushroom-like metasurface, a novel hybrid metamaterial-based design mechanism is proposed. This proposed hybrid metasurface not only realizes a miniaturized size but also achieves stable wideband broadside radiation by introducing the dual-mode resonance.

To further explain the working principle of the proposed hybrid metasurface, its equivalent circuit is summarized, as shown in Fig. 4. In detail, the conventional DR can be considered as an *RLC* resonant tank [27]. L_d and C_d represent the equivalent inductance and capacitance of the resonator model, respectively. R_d represents the radiation resistance of the DR antenna. The mushroom-like metasurface can be seen as a composite right/left-handed transmission line (CRLH-TL)-based equivalent circuit model with a radiation resistance (R_m) [28]. L_R and C_R are contributed by the right-handed (RH) small patch units. C_L and L_L come from the left-handed (LH) capacitive gaps and LH shorting vias, respectively. The coupling between the DR and mushroom-like metasurface resonator is demonstrated by a coupling capacitor (C_c). Besides, this hybrid metasurface antenna is excited by a slot-coupled feeding structure. Thus, the feeding structure is modeled by a π-type capacitance circuit (C_1 and C_2). The simulated $|S_{11}|$ for the proposed hybrid metasurface obtained by EM simulation and ADS circuit simulation is shown in Fig. 4(b), respectively. The resonance modes from the EM model and the equivalent circuit model are very consistent. The impedance matching difference between EM and circuit models is mainly caused by the parasitic effect

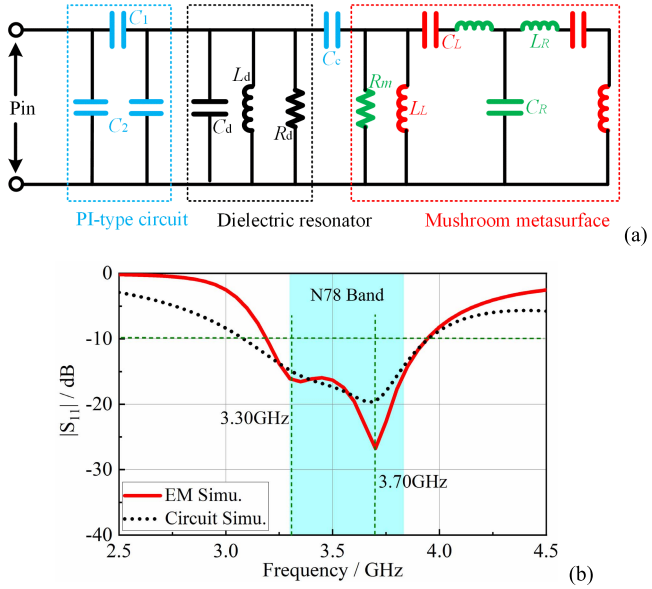

Fig. 4. (a) Equivalent circuit model for the proposed antenna. (b) Simulated $|S_{11}|$ for the hybrid metasurface antenna by using EM simulation and circuit model simulation. The circuit parameters are given as follows: $C_1 = 18.0$ pF, $C_2 = 0.01$ pF, $C_d = 1.40$ pF, $L_d = 0.95$ nH, $R_d = 75\ \Omega$, $C_c = 0.70$ pF, $R_m = 37\ \Omega$, $C_L = 1.04$ pF, $C_R = 2.0$ pF, $L_L = 0.9$ nH, and $L_R = 1.08$ nH.

of the microstrip structure. More importantly, these resonant modes for the proposed hybrid metasurface can be well controlled based on the equivalent circuit model [in Fig. 4(a)]. It agrees with the analysis shown in Fig. 3. In addition, a wide bandwidth response can be easily realized by tuning the coupling (C_c) between the dual modes.

Fig. 5 shows the simulated electric field (E-field) distribution and current distribution for the proposed hybrid metasurface at 3.30 and 3.70 GHz. The classical TE_{111} mode field distribution of the DR is clearly observed [23], as shown in Fig. 5(a). Besides, the surface current is evenly distributed in the metasurface, as shown in Fig. 5(c). At 3.70 GHz (metasurface mode), its E-field distribution is mainly concentrated in the gaps of the hybrid metasurface, and a uniform current loop is observed, as shown in Figs 5(b) and (d), which are similar to the fundamental mode of the classical mushroom-type metasurface [26]. What is more, the in-phase field distributions are excited in both the two modes. Therefore, a stable radiation pattern with the same polarization can be maintained in the whole passband.

To understand the effect of the key geometric dimensions, Fig. 6 shows a parametric study for the proposed hybrid metasurface antenna. With reference to Fig. 6(a), two resonance modes shift to the lower region, as the height of the DR (h) increases. The result shows that L_d and L_L are increased by increasing h. However, only higher resonance is obviously changed, and the lower mode shifts only slightly when g tunes, as shown in Fig. 6(b). This is due to that varying g mainly affects the LH capacitor (C_L) of the mushroom-like metasurface. These results are well proven by its equivalent circuit model [in Fig. 4(a)]. As shown in Fig. 6(c), a wideband dual-mode response with good impedance matching can be easily obtained by tuning the length of the coupled feeding

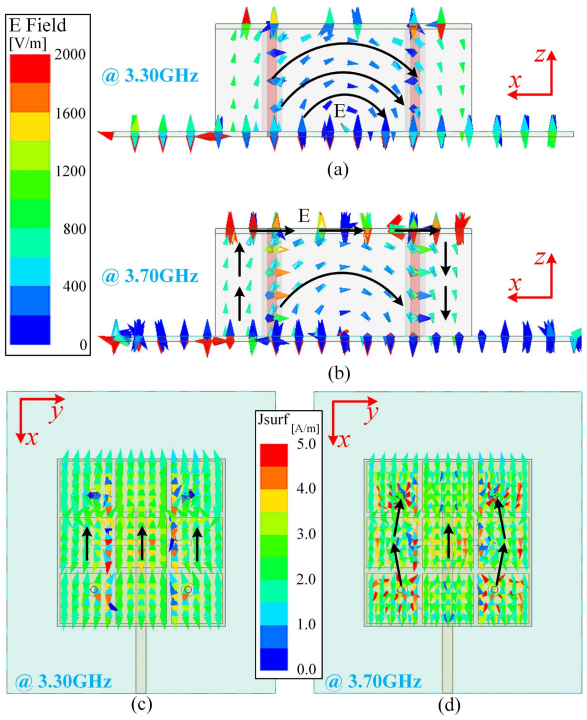

Fig. 5. Simulated E-field distribution and current distribution for the proposed hybrid metasurface antenna at different resonant frequencies. E-field distribution: (a) 3.30 and (b) 3.70 GHz. Surface current distribution: (c) 3.30 and (d) 3.70 GHz.

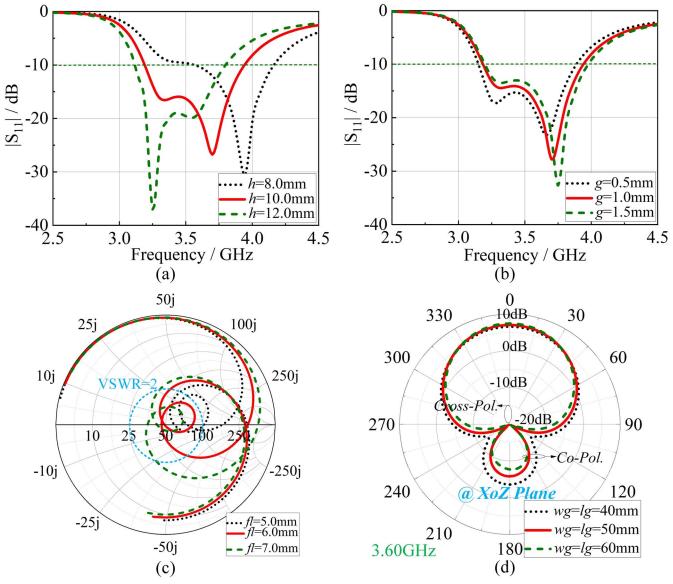

Fig. 6. Parametric study for the proposed hybrid metasurface antenna by varying key parameters. (a) $|S_{11}|$ by varying h. (b) $|S_{11}|$ by varying g. (c) Smith chart by varying fl. (d) Radiation pattern by varying ground size ($wg = lg$).

microstrip line (fl). Besides, the simulated radiation pattern at 3.60 GHz with different ground sizes ($w = l$) is displayed, as shown in Fig. 6(d). The radiation pattern changes slightly by varying w & l. The main reason for this phenomenon is that its radiated field is mainly distributed on the surface of the hybrid metasurface, as shown in Fig. 5. More importantly, since the ground size has little effect on its radiation pattern, the array space between array elements could be flexibly controlled to realize an optimized beam-scanning angle. This excellent characteristic is adopted in the latter (wide-angle beam-scanning phased array design).

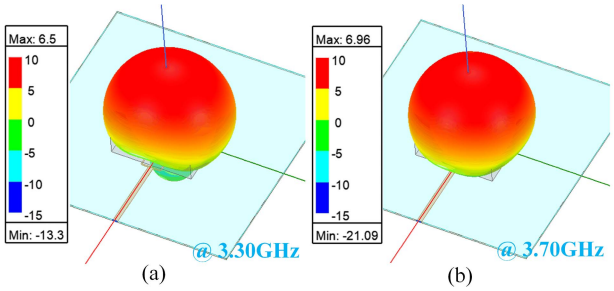

Fig. 7. Simulated 3-D radiation patterns for the proposed hybrid metasurface antenna at different resonant frequencies: (a) 3.30 GHz. (b) 3.70 GHz.

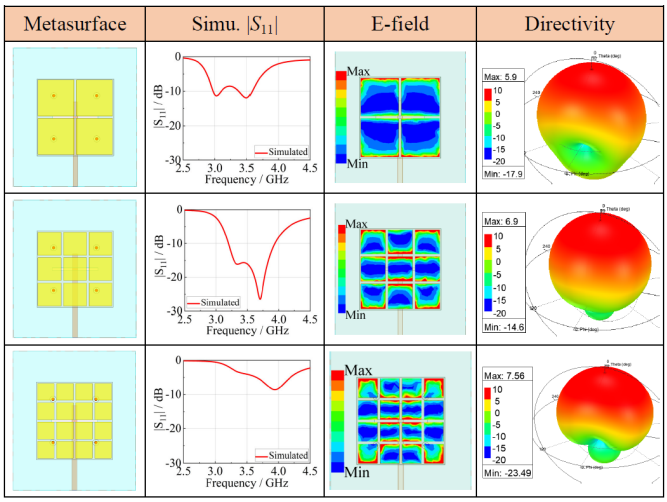

Fig. 8. Comparison of a 2 × 2 mushroom-loaded hybrid metasurface, a 3 × 3 hybrid metasurface, a 4 × 4 hybrid metasurface, and their corresponding simulated $|S_{11}|$, E-field distribution, and radiation directivity-based radiation pattern.

Fig. 7 shows the simulated 3-D radiation pattern for the proposed hybrid metasurface antenna at 3.30 and 3.70 GHz. At the same time, the broadside radiation pattern with roughly equal radiation gain is observed at two resonant modes, respectively. The proposed hybrid metasurface realizes stable broadside radiation in the whole passband. These results are well verified by its in-phase E-field and current distributions, as shown in Fig. 5.

Fig. 8 shows the simulated $|S_{11}|$, E-field distribution, and radiation directivity for different hybrid metasurface structures. In 2 × 2 metasurface form, the lower resonance frequency is observed due to the larger shunt RH-handed capacitance (C_R). Besides, since the number of metasurface gaps (capacitance gaps) reduces, both the radiation aperture and antenna directivity are decreased. Although the 2 × 2 form can help to reduce the size, it suffers from a lower radiation gain. The 4 × 4 metasurface achieves a uniform field distribution

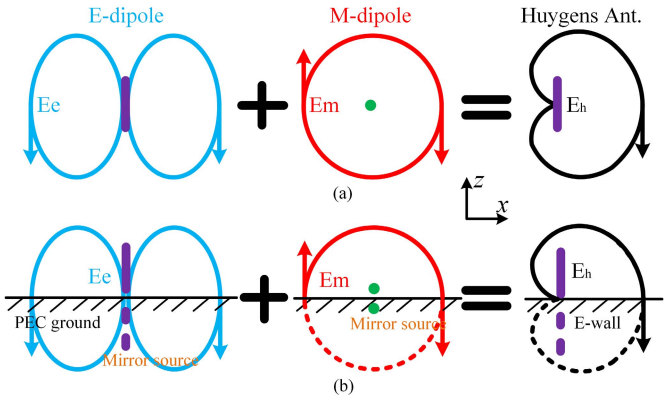

Fig. 9. Basic principle of the Huygens antenna. (a) Huygens principle. (b) Monopole-like Huygens principle. E_e/E_m: Electric fields of the E-dipole and the M-dipole, respectively. E_h is the resultant electric field of the Huygens antenna.

(larger radiation aperture) and a larger radiation directivity by introducing more capacitance gaps. However, its resonance frequency shifts to the high-frequency region due to the smaller shunt RH-handed C_R. Compared with the 2 × 2 and 4 × 4 forms, the 3 × 3 metasurface not only realizes miniaturization and broadband response but also leads to a good radiation directivity. Therefore, the 3 × 3 form is the best choice to realize optimal performance (compact size, broadband, and good radiation capacity).

Generally speaking, due to the mushroom-like metasurface, the novel hybrid metasurface structure not only reduces the size but also expands the bandwidth. It helps to realize a compact Huygens pattern reconfigurable antenna and a wide-angle beam-scanning array.

B. Pattern Reconfigurable Antenna Based on Monopole-Like Huygens Principle

To realize pattern switching for the proposed hybrid metasurface, the Huygens principle is utilized. As shown in Fig. 9(a), a classical Huygens principle is illustrated by using one symmetrical electric dipole (E-dipole) and one small magnetic dipole (M-dipole) [29], [30]. A directional (endfire) pattern without a back lobe is realized. In order to further miniaturize the size and obtain rich multibeam switching capacity, a monopole-like Huygens principle is first proposed. As shown in Fig. 9(b), by introducing a metallic ground layer (PEC surface/electric wall), a monopole radiator with a half-size replaces the symmetrical electric dipole, as the new E-dipole, which is based on the basic mirror principle [31]. Similarly, the original current loop (magnetic dipole) can be replaced by a half-size small loop with its mirror source (new M-dipole). It is worth saying that the new M-dipole radiates a broadside pattern rather than the omnidirectional beam due to the reflection of the ground, which is similar to the vertical split-ring resonator-based antenna [32]. Therefore, a linearly polarized (LP) tilted directional radiation pattern with a large front-to-back (F/B) ratio is obtained, as shown in Fig. 9(b). Furthermore, the tilted direction of the main beam can be selected by tuning the phase difference between the E-dipole and the M-dipole [33], which can be used to implement an LP multibeam antenna or pattern reconfigurable antenna design.

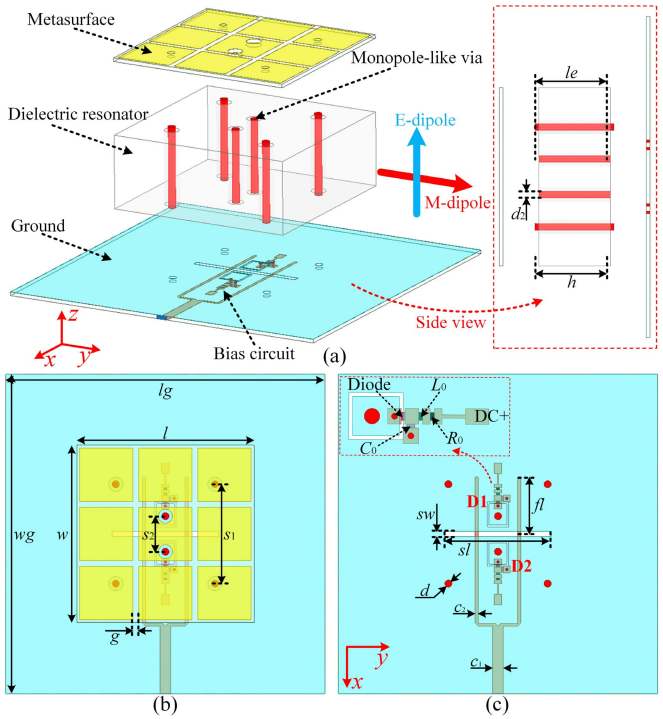

Fig. 10. Configuration of the proposed pattern reconfigurable hybrid metasurface antenna. (a) 3-D view. (b) Top view. (c) Top view without the top layer. (d) Equivalent circuit model of the p-i-n diode.

TABLE I
DIMENSIONS OF THE PROPOSED ANTENNA (mm)

wg	*lg*	*w*	*l*	*g*	s_1	s_2	*h*
50	50	25	25	0.8	14	5	10
le	*d*	d_2	*sl*	*sw*	c_1	c_2	*fl*
10	1.0	1.0	15	0.8	1.5	0.42	6.0

Based on the monopole-like Huygens principle, a pattern reconfigurable hybrid metasurface antenna is proposed, as shown in Fig. 10. The detailed size parameters are listed in Table I. In order to avoid overlapping the feeding microstrip line and the bias circuits of the p-i-n diode (MA4AGP907), a T-shaped coupling feeding structure is implemented on the ground layer, as shown in Fig. 10(a). To realize pattern reconfigurability, two metallic vias with the p-i-n diode (*monopole-like via*) are loaded on both sides of the coupled slot. The dc bias circuits of two p-i-n diodes are printed on the bottom layer of the ground, as shown in Fig. 10(c). In detail, a lumped inductor ($L_0 = 56$ nH) and a capacitor ($C_0 = 100$ pF) are used to isolate the RF signal and dc source, respectively. A series resistor ($R_0 = 100\ \Omega$) is used to limit the current magnitude of the dc bias circuit. The equivalent circuit model of the p-i-n diode is shown in Fig. 10(d), and it is referenced in EM simulation. Note that the slot-coupled feeding structure not only excites a directional M-dipole mode (along the y-direction) but also successfully couples and generates an omnidirectional E-dipole mode (in the z-direction) [34]. Here,

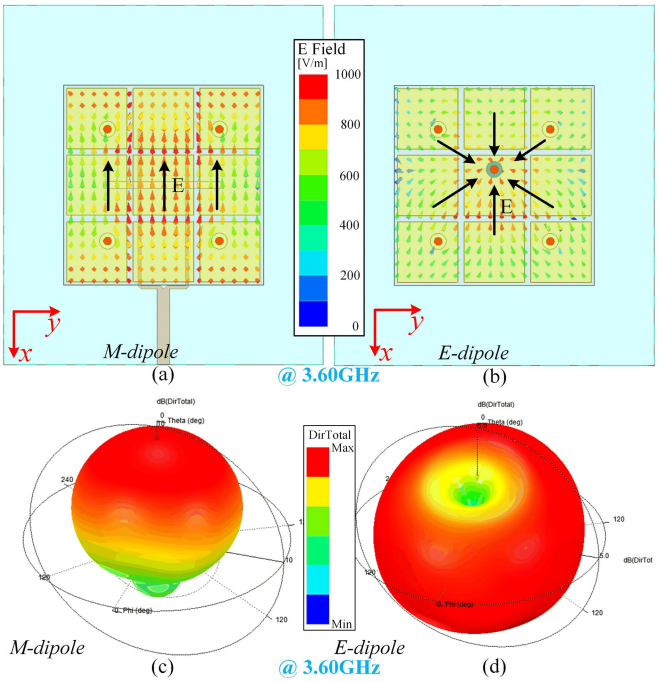

Fig. 11. Simulated E-field distribution and radiation directivity for the proposed Huygens antenna with M-dipole or E-dipole. E-field distribution: (a) M-dipole and (b) E-dipole. Radiation directivity: (c) M-dipole and (d) E-dipole.

a wideband pattern reconfigurable metamaterial-based antenna with a compact size of $0.28\lambda_0 \times 0.28\lambda_0 \times 0.11\lambda_0$ (λ_0 is the free space wavelength at 3.30 GHz) is well implemented.

To further verify the working mechanism, the equivalent M-dipole and E-dipole modes of the proposed hybrid metasurface antenna are studied, as shown in Fig. 11. By using the coupled feeding structure, the dual-mode response (TE_{111} mode and mushroom-like metasurface mode) with equal magnitude and the same polarization for the hybrid metasurface is well excited. The dual-mode response realizes a ring-shaped E-field distribution (odd mode) and a broadside pattern, as shown in Fig. 11(a) and (c), which are similar to a magnetic current source (small loop) on the metallic ground. Therefore, the dual-mode formed resonator can be considered as a y-direction arranged M-dipole. As shown in Fig. 11(b) and (d), the electric monopole mode (E-dipole) for the hybrid metasurface is introduced by loading a shorting via on the DR (Monopole-like via), and a monopole-like field distribution (even mode) and an omnidirectional pattern are observed. Thus, this monopole-like mode provides the required equivalent z-directed E-dipole. The omnidirectional pattern has some slight distortions due to the asymmetric field distribution. Note that, in the proposed reconfigurable design (in Fig. 10), the M-dipole is directly excited by the slot-coupled feeding structure, and the E-dipole (monopole) is successfully coupled by the E-field of the feeding slot. By combining the M-dipole mode and the E-dipole mode, an equivalent monopole-like Huygens source is formed. A tilted directional pattern is operated, as shown in Fig. 8(b).

To realize switchable patterns, two monopole-like vias with the switch (D1 or D2) are loaded on each side of the coupling slot, as shown in Fig. 10(c). When the switch (D1) has turned on the ON-state and D2 is OFF (S1 state), the rear monopole-like via (in the $-x$-axis) is driven, and an equivalent z-directed E-dipole is obtained. Thus, a tilted directional pattern ($\theta = +40°$) is realized based on Fig. 8(b). On the contrary, another tilted pattern ($\theta = -40°$) is switched when the D1 is OFF and the D2 is ON (S3 state). Besides, when both D1 and D2 are OFF (S2 state), two monopole-like vias are not driven, and only the M-dipole mode is excited, leading to a broadside beam ($\theta = 0°$). Therefore, multiple radiation modes ($\theta = -40°$, $0°$, and $+40°$) can be switched by controlling the switches, as shown in Table II.

TABLE II
TUNING STATES OF THE PROPOSED ANTENNA

States	D1	D2	Radiation
S1	ON	OFF	$+x$-direction ($\theta = 40°$)
S2	OFF	OFF	Broadside ($\theta = 0°$)
S3	OFF	ON	$-x$-direction ($\theta = -40°$)

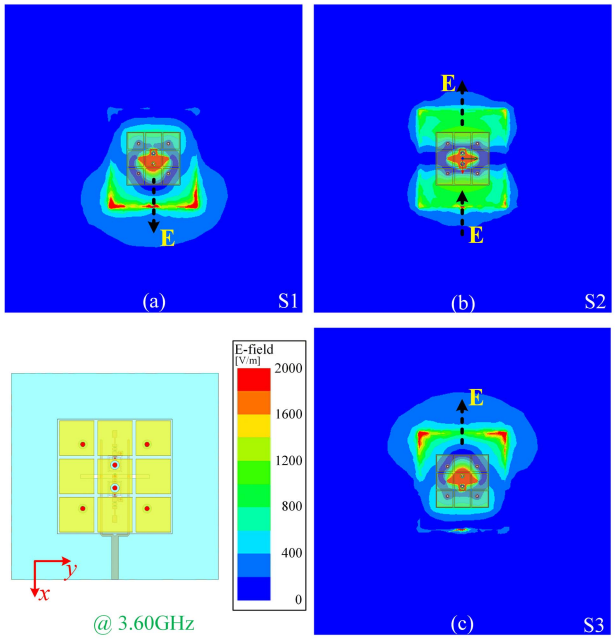

Fig. 12. Simulated E-field distribution of the proposed pattern reconfigurable antenna with different states at 3.60 GHz. (a) S1. (b) S2. (c) S3.

Fig. 12 shows the simulated E-field distribution for the proposed pattern reconfigurable hybrid metasurface antenna at 3.60 GHz with different states. In the S1 state, since one y-directed (x-polarized) M-dipole and one z-directed E-dipole are simultaneously excited, the backward E-field distribution (in the $-x$-axis) is canceled out based on the Huygens principle. The E-field is mainly distributed in the front of the hybrid metasurface, so a frontward tilted beam is realized, as shown in Fig. 12(a). By reversing the switch states, a similar phenomenon (S3 state) is also observed in Fig. 12(c). When both of the two switches are OFF (S2 state), a symmetrical and in-phase E-field distribution is observed in Fig. 12(b). This phenomenon is also similar to a classical half-wavelength

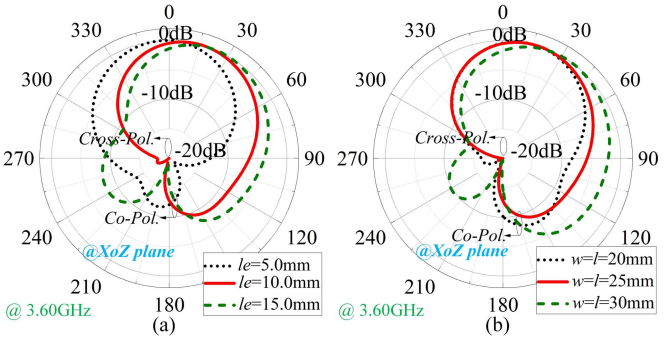

Fig. 13. Simulated radiation pattern of the proposed pattern reconfigurable hybrid metasurface antenna at S1 state by (a) varying *le* and (b) varying DR size ($w = l$).

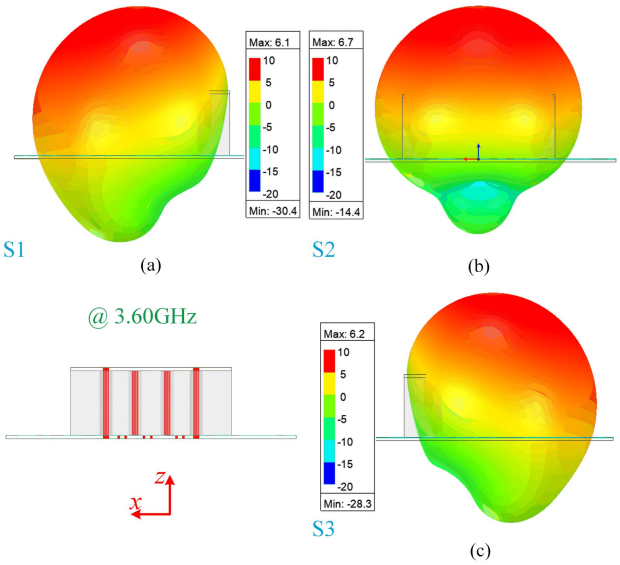

Fig. 14. Simulated 3-D radiation patterns for the proposed pattern reconfigurable antenna with different states at 3.60 GHz: (a) S1, (b) S2, and (c) S3.

patch antenna, so a broadside pattern is achieved [35]. In short, the proposed pattern reconfigurable Huygens antenna can realize LP multibeam switching in the *XoZ* plane by controlling the OFF-/ON-states of two p-i-n diodes.

Fig. 13 shows a parametric study on the simulated pattern for the proposed pattern reconfigurable metasurface antenna to further elaborate the reconfigurable principle. As shown in Fig. 13(a), by increasing the length of the monopole-like via (*le*) from 5.0 to 15.0 mm, the magnitude of the E-dipole component is increased, and the tilted angle of its main beam is also synchronously increased. The influence of the width (length) of the DR ($w = l$) is shown in Fig. 13(b). It is shown that the value variation of $w(l)$ affects the tilted angle. With the increase in the DR dimension from 20.0 to 30.0 mm^2, the magnitude of the M-dipole component is adjusted, and the tilted angle is enlarged from 16° to 45°, which is well proven by the Huygens principle. To sum up, the optimized tilted angle of the main beam can be selected by tuning the size of the M-dipole and E-dipole modes.

Fig. 14 shows the simulated 3-D radiation pattern for the proposed pattern reconfigurable metasurface antenna at

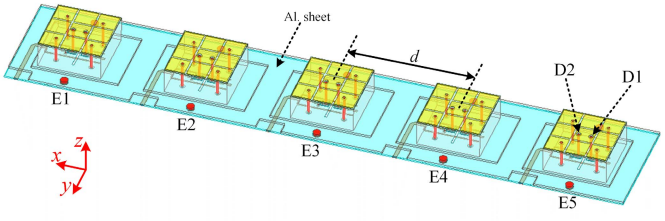

Fig. 15. Geometry of the proposed hybrid metasurface pattern reconfigurable wide-angle beam-scanning phased array.

3.60 GHz with different states. It is clearly observed that the main-lobe direction of the proposed reconfigurable antenna can be tuned among +40°, 0°, and −40° by controlling the OFF-/ON-states of two p-i-n diodes. Besides, the power in the back-lobe direction is much lower than that in its main-lobe direction, as expected. Since the proposed pattern reconfigurable hybrid metasurface antenna has the advantages of wide bandwidth, switchable beams, and simple design, it can be very suitable for 5G wide-angle beam-scanning array, MIMO system, and diversity/multifunction microcell applications.

III. Hybrid Metasurface Array Design

A. Metasurface Low-Cost, Wide-Angle Beam-Scanning Array

To further meet the demands and solve the challenges of the 5G base station in complex application scenarios, a compact low-cost, wide-angle beam-scanning array using the pattern reconfigurable hybrid metasurface elements is designed and implemented, as shown in Fig. 15. Based on the application scenario and low-cost requirement, a five-element linear array is developed and fabricated. The array space between the elements (d) is set to be $0.50\lambda_0$ (50 mm). The total dimension of the proposed reconfigurable phased array is 245 mm × 50 mm × 10 mm ($2.45\lambda_0 \times 0.50\lambda_0 \times 0.11\lambda_0$ only). Here, a 0.8 mm-thick aluminum sheet is fastened to the ground layer for the proposed array, which enhances the mechanical strength and is easy to install. It is also pointed out that, since the array element has three switchable pattern modes (S1/S2/S3), the proposed phased array can realize continued wide-angle beam scanning by switching different pattern modes, as shown in Table III. Note that, in order to balance the size reduction and wide-angle beam-scanning range, the tilted angle of the main lobe of the proposed pattern reconfigurable array element is determined to be [−40°, 0°, +40°]. Therefore, the proposed reconfigurable phased array can easily extend the beam-scanning region from ±35° (A2 state) to ±70° by using the tilted pattern elements (A1/A3 state). The prototype of the metamaterial-based wide-angle beam-scanning array is fabricated and evaluated.

B. Simulation and Discussion

Fig. 16 shows the simulated *E*-field distribution of the proposed metamaterial-based array at 3.60 GHz with different array states. In state A1, the switch (D1) of every element (E1-5) has turned on the ON-state, and all D2s are in OFF-state;

TABLE III
BEAM-SCANNING STATES OF THE PROPOSED ARRAY

State	Array	Switches	Scan
A1	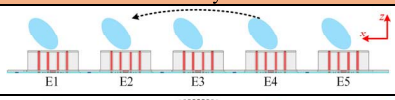	D1 (ON) D2 (OFF)	$+x$
A2	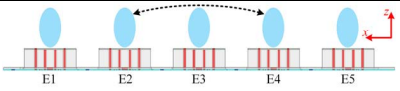	D1 (OFF) D2 (OFF)	[$-x$, x]
A3	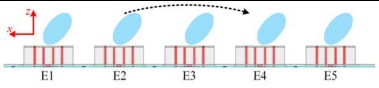	D1 (OFF) D2 (ON)	$-x$

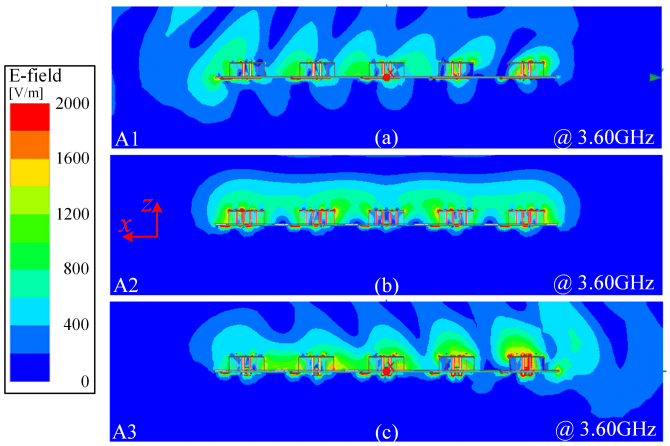

Fig. 16. Simulated E-field distribution of the proposed hybrid metasurface wide-angle beam-scanning phased array with different states at 3.60 GHz. (a) A1 state with $\delta\varphi = -220°$. (b) A2 state with $\delta\varphi = 0°$. (c) A3 state with $\delta\varphi = 220°$.

the main-lobe direction of the original radiation pattern of every element (θ) is about $+40°$. When the feeding phase difference between elements ($\delta\varphi$) is $-220°$, a $+70°$ tilted beam with a peak gain of 11.5 dBi is realized, and a $+x$-directed tilted E-field distribution of this array is clearly observed, as shown in Fig. 16(a). In Fig. 16(b) (A2 state), the switches (D1 and D2) for every element have turned on the OFF-state, the main-lobe direction of the original radiation pattern of the element (θ) is 0°. When the feeding phase difference between elements ($\delta\varphi$) is 0°, a broadside pattern ($\theta = 0°$) with a peak gain of 12.7 dBi is realized. Meanwhile, a uniform and in-phase field distribution is also clearly observed, as shown in Fig. 16(b). In state A3, the switch (D1) of every element (E1-5) is OFF, and all D2s are turned on; the main-lobe direction of the original radiation pattern of every element (θ) is $-40°$. On the contrary, when the feeding phase difference between elements ($\delta\varphi$) is 220°, a $-70°$ tilted beam with a peak gain of 11.5 dBi is obtained, and a -x-directed tilted field distribution is clearly observed, as shown in Fig. 16(c). Generally speaking, the beam-scanning angle or direction for the proposed array can be well controlled by its surface field distribution.

Importantly, every array element has three pattern states ($-40°$, 0°, and $+40°$), so the wide-angle beam-scanning function is realized by combining three different scanning regions (A1, A2, and A3), as shown in Fig. 17. Note that, in order

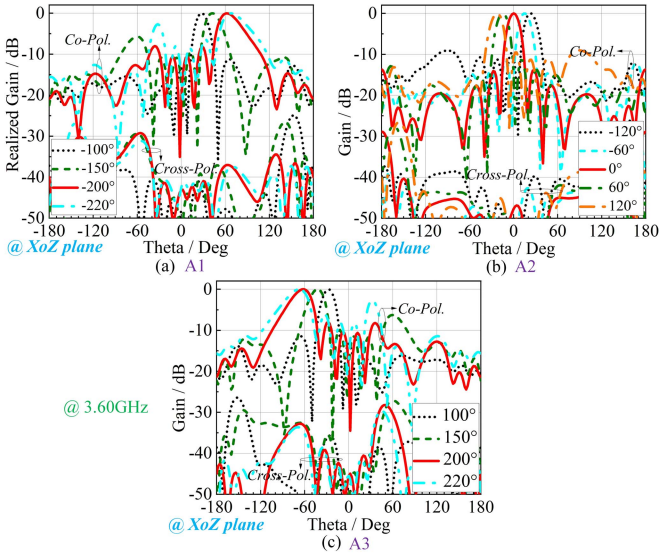

Fig. 17. Simulated scanning beam for the proposed hybrid metasurface phased array with varied feeding phase differences at 3.60 GHz. (a) A1 state. (b) A2 state. (c) A3 state.

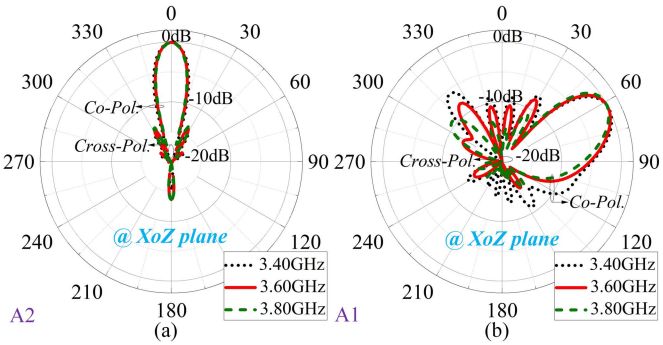

Fig. 18. Simulated radiation patterns for the proposed hybrid metasurface phased array with different states at 3.40/3.60/3.80 GHz for (a) A2 state and (b) A3 state.

to simplify the control and effectively verify the proposed working principle, only the feeding phase difference for the proposed phased array (Phase only) is adjusted. As shown in Fig. 17(a), the beam-scanning region (θ) for the main beam direction is from $+35°$ to $+70°$ by tuning the feeding phase difference ($\delta\varphi$) from $-100°$ to $-220°$. In state A2, the beam-scanning region for the main beam direction is from $-35°$ to $+35°$ by tuning the feeding phase difference from $-120°$ to 120°, as shown in Fig. 17(b). In the final state (A3 state), by tuning the feeding phase difference from 100° to 220°, the beam scanning region covers from $-35°$ to $-70°$ well, which is observed in Fig. 17(c). Note that the side- and back-lobe levels for the large-angle beam-scanning condition are slightly larger. This phenomenon can be well improved by adjusting the port magnitude of the array elements (amplitude control) or increasing the number of the array elements in practical applications.

In practical applications, the effective beam-scanning bandwidth for the array is very important, which directly affects the quality of the wireless communication system. To further

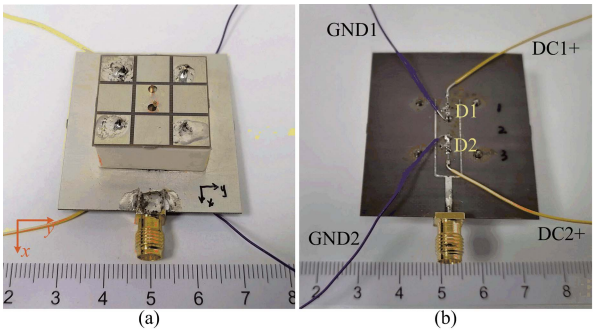

Fig. 19. Photograph of the proposed pattern reconfigurable hybrid metasurface antenna. (a) Top view. (b) Back view.

demonstrate the stability of the scanning beam, Fig. 18 shows the simulated radiation pattern for the proposed metamaterial-based array at 3.40/3.60/3.80 GHz with different array states. The proposed linear array can realize stable and wide-angle beam-scanning capacity with good radiation performance and high polarization purity across the bandwidth from 3.30 to 3.80 GHz.

C. Design Guideline

Based on the mentioned working principles, a general design guideline is summarized as follows.

Step 1: Calculate the rough dimensions of the antenna based on its working frequency and DR theory [36].

Step 2: Determine the number of elements of the proposed hybrid metasurface structure based on the desired size and gain (in Fig. 8).

Step 3: Determine the length of the switchable monopole-like vias (*le*) based on the Huygens principles and the desired tilted beam (in Fig. 13).

Step 4: Select the number of array elements (n) and array space between elements (d) to realize the desired beam scanning region.

Step 5: Optimize the final size parameter of the proposed array by using EM simulation software (HFSS or CST).

Note that steps 2–5 need to be carried out repeatedly to achieve optimal performance.

IV. Measurement and Comparison

A. Array Element Measurement

A pattern reconfigurable hybrid metasurface antenna based on the proposed monopole-like Huygens principle is fabricated and measured, as shown in Fig. 19. To control the OFF-/ON-states of two p-i-n diodes, two dc bias circuits are implemented by using two dc+ signals (yellow line) and two GND signals (purple line), as shown in Fig. 19(b). Note that, to reduce the complexity of the control circuit (p-i-n diode bias circuit), the GND signals of multiple p-i-n diodes can be combined together by using a common ground, especially for array designs.

Fig. 20 shows the measured and simulated $|S_{11}|$ for the proposed hybrid metasurface antenna with different states. The measured overlapped -10 dB impedance bandwidth for the three states is from 3.30 to 3.85 GHz, which well covers the 5G-N78 (3.30–3.80 GHz) band. Besides, two resonant modes are clearly observed in the passband, and its realized bandwidth is wider than that of the original DR antenna with a single mode.

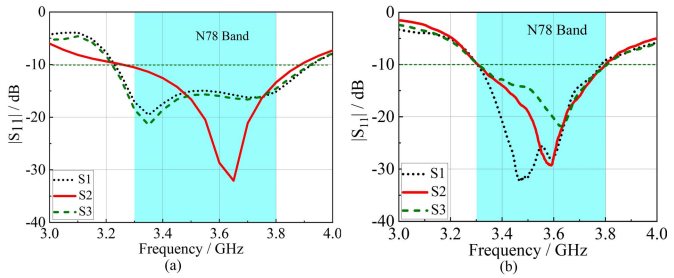

Fig. 20. Simulated and measured $|S_{11}|$ for the proposed pattern reconfigurable hybrid metasurface antenna with different states. (a) Simulated results. (b) Measured results.

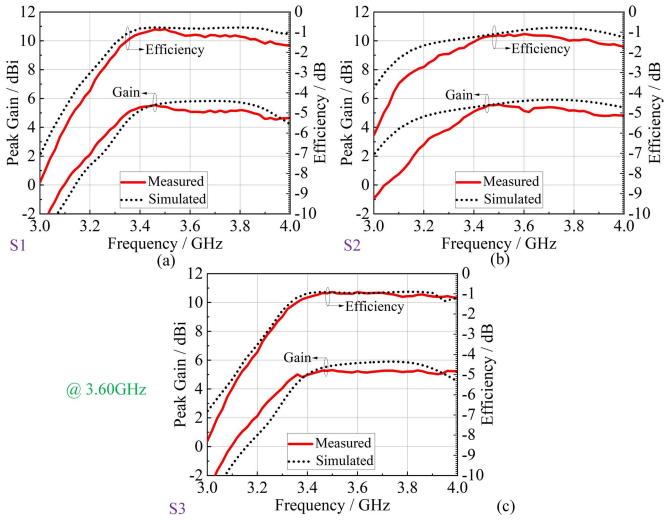

Fig. 21. Simulated and measured peak gains and radiation efficiencies for the proposed pattern reconfigurable hybrid metasurface antenna with different states: (a) S1 state, (b) S2 state, and (c) S3 state.

Fig. 21 shows the measured and simulated peak gain and radiation efficiency for the proposed reconfigurable hybrid metasurface antenna with different states. It is seen that the proposed antenna can realize stable radiation with a peak gain larger than 5.0 dBi and a peak radiation efficiency of greater than -1.05 dB (78.4%) for different modes. Note that the measured results are slightly lower than that in simulation, which is mainly caused by the fabrication tolerance and the extra loss from the SMA connector.

Fig. 22 shows the measured and simulated radiation patterns for the proposed reconfigurable hybrid metasurface antenna at 3.60 GHz with different states. The measured results are in line with the simulation. The proposed reconfigurable metasurface antenna can be operated at $-40°$, $0°$, and $+40°$ tilted pattern modes by switching the OFF-/ON-states of two p-i-n diodes based on Table II, respectively. In addition, the cross-pol. levels for three modes are lower than -15 dB, and their back-lobe levels are also suppressed. Therefore, the proposed pattern

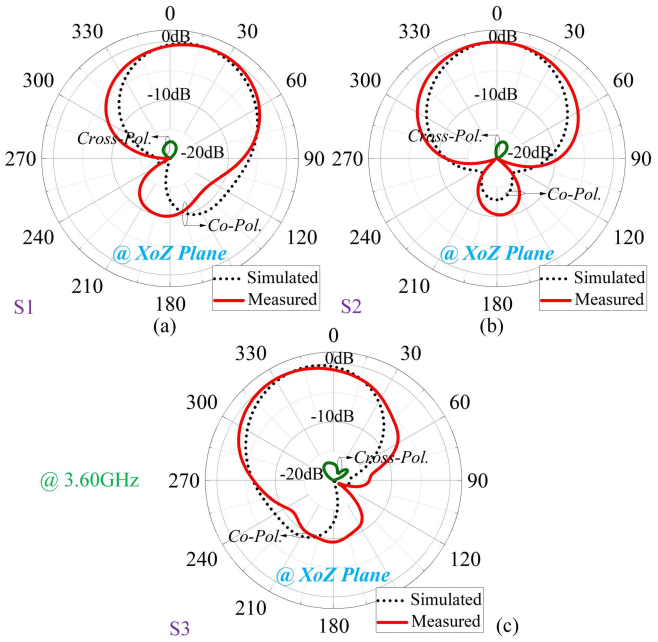

Fig. 22. Simulated and measured radiation patterns for the proposed pattern reconfigurable hybrid metasurface antenna with different states at 3.60 GHz: (a) S1 state, (b) S2 state, and (c) S3 state.

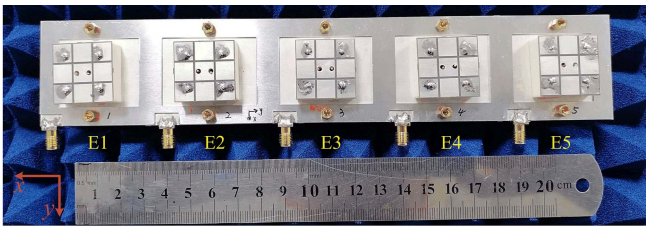

Fig. 23. Photograph of the proposed hybrid metasurface reconfigurable wide-angle beam-scanning phased array.

reconfigurable metasurface antenna with a compact size, wide bandwidth, and flexible beam-scanning capacity is very suitable for space-limited multibeam sub-6 GHz microcell and router applications.

B. Wide-Angle Beam-Scanning Array Measurement

To validate the proposed design principle and working mechanism, a five-element metamaterial-based pattern reconfigurable low-cost, wide-angle beam-scanning linear array is fabricated and tested, as shown in Fig. 23.

Fig. 24 shows the measured and simulated *S*-parameter for the proposed hybrid metasurface linearly array at the A2 state. The proposed hybrid metasurface array works from 3.30 to 3.80 GHz (covering the 5G-N78 band well), which is slightly narrower than that in simulation. The resonance frequencies for every element have a small shift compared with the single pattern reconfigurable hybrid metasurface element, which is due to the coupling between the array elements. The reflection coefficients of the edge elements are slightly different from the center elements because of the edge effect. In addition, the port isolation between the array elements is better than

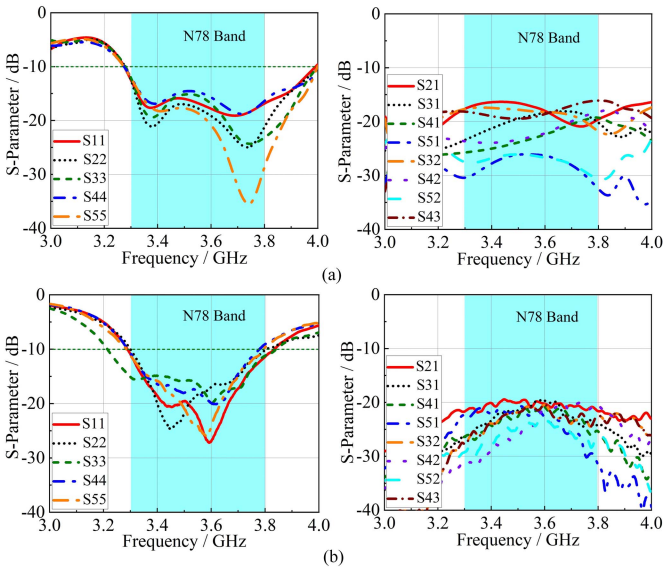

Fig. 24. Simulated and measured *S*-parameters for the proposed hybrid metasurface wide-angle beam-scanning phased array at the A2 state. (a) Simulated results. (b) Measured results.

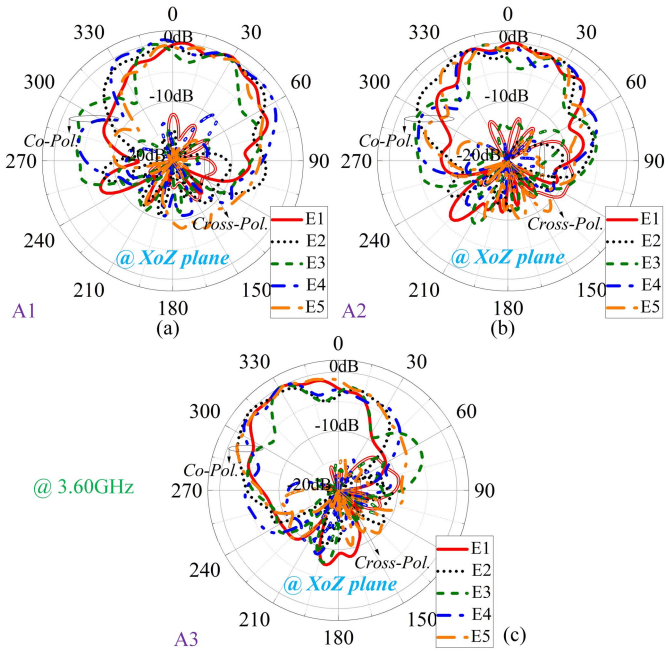

Fig. 25. Measured radiation patterns of the active element of the proposed hybrid metasurface wide-angle beam-scanning phased array with different states at 3.60 GHz: (a) A1 state, (b) A2 state, and (c) A3 state.

18 dB in the whole passband. Note that, based on the reflection coefficient for the single pattern reconfigurable antenna (in Fig. 20) and good port isolation between array elements, similar *S*-parameter curves are also observed at A1 and A3 states. Therefore, only the *S*-parameter at state A2 is shown here.

The beam-scanning angle (θ) for the proposed phased array is determined by the active array element radiation patterns with the effects of mutual coupling. The active array element

TABLE IV
COMPARISON WITH THE PREVIOUS WORKS

Ref.	Technology	Size \ λ_0^3	Num. element	BW / %	Scanning angle	Gain / dBi	Remark
[37]	Slot-coupled feeding metasurface	5.69×1.12×0.05	7	23.1	[-50°, 50°]	11.9	Narrow scanning region; more array elements
[13]	Phase gradient metasurface	9.29×2.06×0.51	6	3.0	[-56°, 60°]	9.5	Narrow BW; large dimension; limited scanning region
[38]	Reconfigurable Yagi-like ant.	3.37×0.44× 0.25	5	6.2	[-70°, 70°]	7.8	High profile; large size low radiation gain
[14]	Reconfigurable magnetic current element	3.81× 2.20×0.19	8	5.2	[-75°, 75°]	15.5	Complex structure; more elements; limited BW
[39]	Pattern diversity dielectric resonator ant.	2.0×0.40×0.26	4	3.33	[-81°, 81°]	7.2	High profile; narrow BW; poor scanning capacity
[40]	Four-folded-dipole; Dual-polarized ant.	1.0×4.87×0.52	6	64.7	Fixed beam	13.7	Wideband; high profile, large dimension
[41]	Differentially fed. dual-band patch ant.	2.76×0.75×0.13	4	11.7 / 7.6	Fixed beam	13.5	Fixed beam; complex structure; large size
[42]	Crossed dipole ant. with cavity-backed structure	2.80×2.80×0.26	4×4	13.0	[-45°, 45°]	15.8	High profile; limited beam-scanning capacity
Prop.	Hybrid metasurface; Huygens reconfigurable element	2.45×0.50×0.11	5	14.1	[-70°, 70°]	10.5	Compact size; broadband; continuously wide-angle scanning

pattern is obtained by driving one array element and matching other array elements with 50 Ω resistors [11]. The measured radiation patterns for every active element at three states (A1, A2, and A3) in the E-plane (in the *XoZ* plane) at 3.60 GHz are shown in Fig. 25, respectively. As shown in Fig. 25(a) and (c), the tilted patterns for every element with a low cross-pol. levels of −15 dB are clearly observed, which is in good agreement with the single antenna. In state A2, five broadside patterns with a half-power beamwidth of 90° are shown in Fig. 25(b). Note that the ripple on the pattern is due to the impact of other terminated unit cells.

By selecting the states of p-i-n diodes (A1, A2, and A3) and tuning the feeding phase difference ($\delta\varphi$), the proposed metamaterial-based array can realize wide-angle beam scanning. Fig. 26 shows the measured and simulated radiation patterns for the proposed metamaterial-based array at 3.60 GHz. It is clearly seen that the main beam with a low cross-pol. levels can be continuously steered from −70° to +70° in the E-plane. The measured beam-scanning angle has now been extended to a wide range from [−35°, +35°] to [−70°, +70°] due to the reconfigurable multibeam working mechanism. Besides, the measured peak gain for the proposed phased array is greater than 11.4 dBi. Note that the measured realized gain is slightly lower than the simulated results, which is mainly due to the fabrication tolerance, the extra loss from SMA connectors, and the parasitic effects of the bias circuits. In other words, the proposed pattern reconfigurable metamaterial-based phased array can bidirectionally move the beam of the conventional array to a wider region, which makes it suitable for low-cost multibeam base stations and phased array systems.

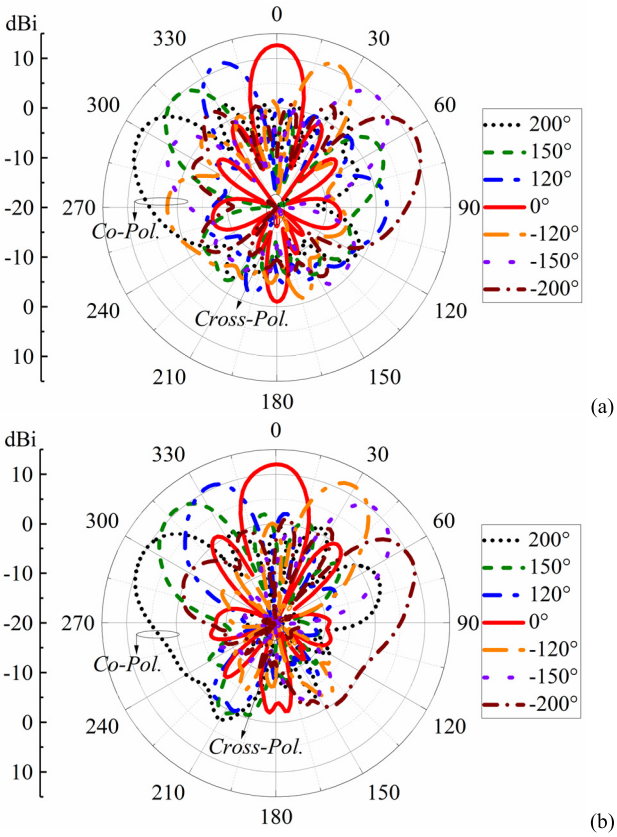

Fig. 26. Simulated and measured beam-scanning results for the proposed hybrid metasurface wide-angle beam-scanning phased array at 3.60 GHz. (a) Simulated results. (b) Measured results.

C. Comparison With the Previous Works

A comprehensive comparison between the proposed metamaterial-based wide-angle beam-scanning array and the reported wide-angle beam-scanning arrays and the previous base station antennas is given in Table IV. Two metasurface-based array antennas were proposed in [13] and [37], but their beam-scanning range is limited, and they require more elements (higher cost). Compared with two conventional pattern reconfigurable beam-scanning arrays [14], [38], the proposed design has a wider bandwidth, more compact size, and a simple design (low-cost). Recently, the work in [39]

presented a DR-based phased array, but it suffers from a narrow bandwidth, high profile, and limited continuously beam-scanning capacity. The proposed design realizes a more compact size, flexible beam-switching/ scanning function, and wide-angle coverage capacity, compared with other base station antennas [40]–[42].

Compared with the conventional works, the proposed design exhibits a compact size, low cost (simple design and fewer elements), and wide bandwidth ($>14.1\%$) while yielding a wide beam-scanning region of $[-70°, +70°]$ and good radiation properties, which verifies that it is a competitive candidate for 5G base station and microcell applications. Besides, this novel work enables or opens a new application direction for hybrid metamaterials.

V. Conclusion

In this study, a novel hybrid metasurface, DR, low-cost, wide-angle beam-scanning antenna/array with the Huygens pattern reconfigurable element is proposed for the 5G application. An aperture-shared hybrid metasurface with a broad bandwidth of 15.4% is first proposed, which is designed as a Huygens-based pattern reconfigurable antenna. A low-cost, wide-angle beam-scanning array is realized by using multiple pattern reconfigurable elements. To demonstrate the idea, a five-element phased array with an array space of $0.5\lambda_0$ is fabricated and measured. The proposed phased array can realize a continuous beam-scanning region from $-70°$ to $+70°$ by tuning the feeding phase difference. The proposed wide-angle beam-scanning phased array as a novel hybrid metamaterial application has the advantages of compact size, broadband, low cost (simple design and fewer elements), and wide beam-scanning range. It is very suitable for 5G base stations, radar, and positioning systems.

References

[1] K. M. Mak, H. W. Lai, and K. M. Luk, "A 5G wideband patch antenna with antisymmetric L-shaped probe feeds," *IEEE Trans. Antennas Propag.*, vol. 66, no. 2, pp. 957–961, Feb. 2018.

[2] C. X. Mao, M. Khalily, P. Xiao, T. W. C. Brown, and S. Gao, "Planar sub-millimeter-wave array antenna with enhanced gain and reduced sidelobes for 5G broadcast applications," *IEEE Trans. Antennas Propag.*, vol. 67, no. 1, pp. 160–168, Jan. 2019.

[3] C. Ding, H.-H. Sun, H. Zhu, and Y. J. Guo, "Achieving wider bandwidth with full-wavelength dipoles for 5G base stations," *IEEE Trans. Antennas Propag.*, vol. 68, no. 2, pp. 1119–1127, Feb. 2020.

[4] W. Hong *et al.*, "Multibeam antenna technologies for 5G wireless communications," *IEEE Trans. Antennas Propag.*, vol. 65, no. 12, pp. 6231–6249, Dec. 2017.

[5] J. Park, M. Choo, S. Jung, D. Choi, J. Choi, and W. Hong, "A software-programmable directivity, beamsteering, and polarization reconfigurable block cell antenna concept for millimeter-wave 5G phased-array architectures," *IEEE Trans. Antennas Propag.*, vol. 69, no. 1, pp. 146–154, Jan. 2021.

[6] M. A. Hossain, I. Bahceci, and B. A. Cetiner, "Parasitic layer-based radiation pattern reconfigurable antenna for 5G communications," *IEEE Trans. Antennas Propag.*, vol. 65, no. 12, pp. 6444–6452, Dec. 2017.

[7] C. Gu *et al.*, "3-D coverage beam-scanning antenna using feed array and active frequency-selective surface," *IEEE Trans. Antennas Propag.*, vol. 65, no. 11, pp. 5862–5870, Nov. 2017.

[8] H. Al-Saedi *et al.*, "An integrated circularly polarized transmitter active phased-array antenna for emerging Ka-band satellite mobile terminals," *IEEE Trans. Antennas Propag.*, vol. 67, no. 8, pp. 5344–5352, Aug. 2019.

[9] J.-J. Peng, S.-W. Qu, M. Xia, and S. Yang, "Conformal phased array antenna for unmanned aerial vehicle with $\pm 70°$ scanning range," *IEEE Trans. Antennas Propag.*, vol. 69, no. 8, pp. 4580–4587, Aug. 2021.

[10] V. F. Fusco, "Mechanical beam scanning reflectarray," *IEEE Trans. Antennas Propag.*, vol. 53, no. 11, pp. 3842–3844, Nov. 2005.

[11] C.-M. Liu, S.-Q. Xiao, H.-L. Tu, and Z. Ding, "Wide-angle scanning low profile phased array antenna based on a novel magnetic dipole," *IEEE Trans. Antennas Propag.*, vol. 65, no. 3, pp. 1151–1162, Mar. 2017.

[12] R. Wang, B.-Z. Wang, X. Ding, and X.-S. Yang, "Planar phased array with wide-angle scanning performance based on image theory," *IEEE Trans. Antennas Propag.*, vol. 63, no. 9, pp. 3908–3917, Sep. 2015.

[13] Y.-H. Lv, X. Ding, B.-Z. Wang, and D. E. Anagnostou, "Scanning range expansion of planar phased arrays using metasurfaces," *IEEE Trans. Antennas Propag.*, vol. 68, no. 3, pp. 1402–1410, Mar. 2020.

[14] X. Ding, Y.-F. Cheng, W. Shao, H. Li, B.-Z. Wang, and D. E. Anagnostou, "A wide-angle scanning planar phased array with pattern reconfigurable magnetic current element," *IEEE Trans. Antennas Propag.*, vol. 65, no. 3, pp. 1434–1439, Mar. 2017.

[15] X. Ding, Y.-F. Cheng, W. Shao, and B.-Z. Wang, "A wide-angle scanning phased array with microstrip patch mode reconfiguration technique," *IEEE Trans. Antennas Propag.*, vol. 65, no. 9, pp. 4548–4555, Sep. 2017.

[16] N. R. Labadie, S. K. Sharma, and G. M. Rebeiz, "A novel approach to beam steering using arrays composed of multiple unique radiating modes," *IEEE Trans. Antennas Propag.*, vol. 63, no. 7, pp. 2932–2945, Jul. 2015.

[17] D. Hua, W. Wu, and D.-G. Fang, "Linear array synthesis to obtain broadside and endfire beam patterns using element-level pattern diversity," *IEEE Trans. Antennas Propag.*, vol. 65, no. 6, pp. 2992–3004, Jun. 2017.

[18] Y. He and Y. Li, "Dual-polarized microstrip antennas with capacitive via fence for wide beamwidth and high isolation," *IEEE Trans. Antennas Propag.*, vol. 68, no. 7, pp. 5095–5103, Jul. 2020.

[19] Y. Dong, H. Toyao, and T. Itoh, "Compact circularly-polarized patch antenna loaded with metamaterial structures," *IEEE Trans. Antennas Propag.*, vol. 59, no. 11, pp. 4329–4333, Nov. 2011.

[20] B. P. Smyth and A. K. Iyer, "Low-profile uniplanar dual-band and dual-polarized microstrip patch antenna using embedded MTM-EBGs," *IEEE Trans. Antennas Propag.*, vol. 69, no. 7, pp. 3645–3653, Jul. 2021.

[21] W. Lin and R. W. Ziolkowski, "Electrically small, single-substrate Huygens dipole rectenna for ultracompact wireless power transfer applications," *IEEE Trans. Antennas Propag.*, vol. 69, no. 2, pp. 1130–1134, Feb. 2021.

[22] J. Zhang, S. Yan, and G. A. E. Vandenbosch, "Radial CRLH-TL-based dual-band antenna with frequency agility," *IEEE Trans. Antennas Propag.*, vol. 68, no. 7, pp. 5664–5669, Jul. 2020.

[23] Z. Wang and Y. Dong, "Miniaturized RFID reader antennas based on CRLH negative order resonance," *IEEE Trans. Antennas Propag.*, vol. 68, no. 2, pp. 683–696, Feb. 2020.

[24] W. Liu, Z. N. Chen, and X. Qing, "Metamaterial-based low-profile broadband mushroom antenna," *IEEE Trans. Antennas Propag.*, vol. 62, no. 3, pp. 1165–1172, Dec. 2014.

[25] L. Guo and K. W. Leung, "Compact linearly and circularly polarized unidirectional dielectric resonator antennas," *IEEE Trans. Antennas Propag.*, vol. 64, no. 6, pp. 2067–2074, Jun. 2016.

[26] W. Liu, Z. N. Chen, and X. Qing, "60-GHz thin broadband high-gain LTCC metamaterial-mushroom antenna array," *IEEE Trans. Antennas Propag.*, vol. 62, no. 9, pp. 4592–4601, Sep. 2014.

[27] S.-K. Zhao, N.-W. Liu, Q. Chen, G. Fu, and X.-P. Chen, "A low-profile dielectric resonator antenna with compact-size and wide bandwidth by using metasurface," *IEEE Access*, vol. 9, pp. 29819–29826, 2021.

[28] Y. Dong and T. Itoh, "Miniaturized substrate integrated waveguide slot antennas based on negative order resonance," *IEEE Trans. Antennas Propag.*, vol. 58, no. 12, pp. 3856–3864, Dec. 2010.

[29] L. Guo, K. W. Leung, and Y. M. Pan, "Compact unidirectional ring dielectric resonator antennas with lateral radiation," *IEEE Trans. Antennas Propag.*, vol. 63, no. 12, pp. 5334–5342, Dec. 2015.

[30] Y. M. Pan, K. W. Leung, and L. Guo, "Compact laterally radiating dielectric resonator antenna with small ground plane," *IEEE Trans. Antennas Propag.*, vol. 65, no. 8, pp. 4305–4310, Aug. 2017.

[31] J. Wang *et al.*, "A low-profile vertically polarized magneto-electric monopole antenna with a 60% bandwidth for millimeter-wave applications," *IEEE Trans. Antennas Propag.*, vol. 69, no. 1, pp. 3–13, Jan. 2021.

[32] Z. Wang, Y. Dong, and T. Itoh, "Ultraminiature circularly polarized RFID antenna inspired by crossed split-ring resonator," *IEEE Trans. Antennas Propag.*, vol. 68, no. 6, pp. 4196–4207, Jun. 2020.

[33] M.-C. Tang, H. Wang, and R. W. Ziolkowski, "Design and testing of simple, electrically small, low-profile, Huygens source antennas with broadside radiation performance," *IEEE Trans. Antennas Propag.*, vol. 64, no. 11, pp. 4607–4617, Nov. 2016.
[34] K. Sun, Y. Chen, S. Liu, Y. Zhao, and D. Yang, "Substrate-integrated-waveguide-based complementary source array with enhanced beamwidth," *IEEE Trans. Antennas Propag.*, vol. 69, no. 8, pp. 5136–5141, Aug. 2021.
[35] C. A. Balanis, *Antenna Theory, Analysis and Design*. Hoboken, NJ, USA: Wiley, 2005.
[36] K. M. Luk and K. W. Leung, *Dielectric Resonator Antennas*. Hertfordshire, U.K.: Research Studies Press, 2003.
[37] L. Gu, Y.-W. Zhao, Q.-M. Cai, Z.-P. Zhang, B.-H. Xu, and Z.-P. Nie, "Scanning enhanced low-profile broadband phased array with radiator-sharing approach and defected ground structures," *IEEE Trans. Antennas Propag.*, vol. 65, no. 11, pp. 5846–5854, Nov. 2017.
[38] S. Xiao, C. Zheng, M. Li, J. Xiong, and B.-Z. Wang, "Varactor-loaded pattern reconfigurable array for wide-angle scanning with low gain fluctuation," *IEEE Trans. Antennas Propag.*, vol. 63, no. 5, pp. 2364–2369, May 2015.
[39] Z. Chen, Z. Song, H. Liu, X. Liu, J. Yu, and X. Chen, "A compact phase-controlled pattern-reconfigurable dielectric resonator antenna for passive wide-angle beam scanning," *IEEE Trans. Antennas Propag.*, vol. 69, no. 5, pp. 2981–2986, May 2021.
[40] L. H. Ye, X. Y. Zhang, Y. Gao, and Q. Xue, "Wideband dual-polarized four-folded-dipole antenna array with stable radiation pattern for base-station applications," *IEEE Trans. Antennas Propag.*, vol. 68, no. 6, pp. 4428–4436, Jun. 2020.
[41] Y. Li, Z. Zhao, Z. Tang, and Y. Yin, "Differentially fed, dual-band dual-polarized filtering antenna with high selectivity for 5G sub-6 GHz base station applications," *IEEE Trans. Antennas Propag.*, vol. 68, no. 4, pp. 3231–3236, Apr. 2020.
[42] M. V. Komandla, G. Mishra, and S. K. Sharma, "Investigations on dual slant polarized cavity-backed massive MIMO antenna panel with beamforming," *IEEE Trans. Antennas Propag.*, vol. 65, no. 12, pp. 6794–6799, Dec. 2017.

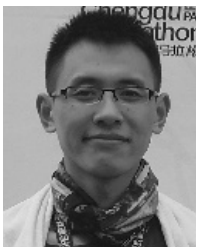

Zhan Wang (Student Member, IEEE) received the B.S. degree in electrical and information engineering (high-speed rail control) from Southwest Jiaotong University (SWJTU), Chengdu, China, in 2018. He is currently pursuing the Ph.D. degree with the University of Electric Science and Technology of China (UESTC), Chengdu, China.

He has published more than 20 papers and five patents. His research interests include miniaturized antennas and microwave devices, especially, metamaterial-based antennas.

Mr. Wang received multiple awards, including multiple national scholarships and the Gold Medal in the 7th "Internet Plus" Innovation and Entrepreneurship Worldwide Competition. He is also serving as a Reviewer for IEEE TRANSACTIONS ON ANTENNAS AND PROPAGATION.

Yuandan Dong (Senior Member, IEEE) received the B.S. and M.S. degrees from the Department of Radio Engineering, Southeast University, Nanjing, China, in 2006 and 2008, respectively, and the Ph.D. degree from the Department of Electrical Engineering, University of California at Los Angeles (UCLA), Los Angeles, CA, USA, in 2012.

From September 2008 to June 2012, he was a Graduate Student Researcher with the Microwave Electronics Laboratory, UCLA. From September 2012 to February 2016, he was a Senior Engineer with the Research and Development Hardware Department, Qualcomm, San Diego, CA, USA. From February 2016 to December 2017, he was a Staff Engineer with Universal Electronics Inc., Santa Ana, CA, USA. Since December 2017, he has been a Full Professor with the University of Electronic Science and Technology of China (UESTC), Chengdu, China. He has authored or coauthored more than 180 journal articles and conference papers, which received more than 4400 citations. He holds more than 70 patents, including six international patents. He and his team have developed multiple RF products, including acoustic wave filters, antenna tuners, and antennas, which are very widely shipped and applied in mobile devices. His research interests include the characterization and development of RF and microwave components, RF modules, circuits, antennas, acoustic-wave filters, and metamaterials.

Dr. Dong has been a TPC member for several international conferences. He was a recipient of the Best Student Paper Award from the 2010 IEEE Asia Pacific Microwave Conference (APMC) held in Yokohama, Japan, the Best Paper Award in the 2021 IEEE International Wireless Symposium (IWS), the Distinguished Expert Presented by Sichuan Province and the China Government, respectively, and the High Level Innovative and Entrepreneurial Talent presented by Jiangsu Province. He is also serving as an Associate Editor for the IEEE TRANSACTIONS ON ANTENNAS AND PROPAGATION and the IEEE OPEN JOURNAL OF ANTENNAS AND PROPAGATION. He is also serving as a Reviewer for multiple IEEE and IET journals, including the IEEE TRANSACTIONS ON MICROWAVE THEORY AND TECHNIQUES and the IEEE TRANSACTIONS ON ANTENNAS AND PROPAGATION.

Zilin Peng received the B.S. degree in electronic information science and technology from the University of Electronic Science and Technology of China (UESTC), Chengdu, China, in 2021, where she is currently pursuing the M.S. degree.

Her research interests include planar antennas and miniaturized antennas for base station applications.

Wei Hong (Fellow, IEEE) received the B.S. degree from the University of Information Engineering, Zhengzhou, China, in 1982, and the M.S. and Ph.D. degrees from Southeast University, Nanjing, China, in 1985 and 1988, respectively, all in radio engineering.

In 1993 and 1995–1998, he was a short-term Visiting Scholar with the University of California at Berkeley, Berkeley, CA, USA, and the University of California at Santa Cruz, Santa Cruz, CA, USA. Since 1988, he has been with the State Key Laboratory of Millimeter Waves, Southeast University, where he is currently a Professor with the School of Information Science and Engineering. He has authored or coauthored over 300 technical publications and two books. He has been engaged in numerical methods for electromagnetic problems, millimeter-wave theory and technology, antennas, RF technology for wireless communications, and so on.

Dr. Hong was an Elected IEEE MTT-S AdCom Member from 2014 to 2016. He is also a fellow of CIE. He was awarded twice the National Natural Prizes, four times awarded the first-class Science and Technology Progress Prizes issued by the Ministry of Education of China and Jiangsu Province Government, and so on. He also received the Foundations for China Distinguished Young Investigators and for "Innovation Group" issued by NSF of China. He is also the Vice-President of the CIE Microwave Society and the Antenna Society, and the Chair of the IEEE MTT-S/AP-S/EMC-S Joint Nanjing Chapter. He has served as an Associate Editor for the IEEE TRANSACTIONS ON MICROWAVE THEORY AND TECHNIQUES from 2007 to 2010.